4^{th} URSI AT-RASC, Gran Canaria, 19 – 24 May 2024

High Data-Rate Sub-THz Coherent Near-Field Wireless Links Enabled by Spline-Profile Bessel Launchers

Jérôme Taillieu[(1)(3)], David González-Ovejero[(1)], Walter Fuscaldo[(2)], Laurent Bramerie[(3)], Paul Desombre[(1)], Mathilde Gay[(3)], Mehdi Alouini[(3)], Haifa Farès[(1)], Yves Louët[(1)] and Mauro Ettorre[(4)]
(1) Univ Rennes & CentralSupélec, CNRS, Institut d'Electronique et des Technologies du numéRique (IETR), Rennes, France
(2) Istituto per la Microelettronica e i Microsistemi, Consiglio Nazionale delle Ricerche, 00133, Roma, Italy
(3) Univ Rennes, CNRS, Institut FOTON, UMR 6082, France
(4) Michigan State University, USA

Abstract

This paper presents a robust high data-rate link using two broadband Bessel beam launchers in the sub-THz range. The carrier is generated by photomixing and photonically modulated, achieving an error-free link at 15.5 Gb/s with QPSK modulation format has been achieved in an offline configuration. Bit Error Rate curves at 2.75 Gb/s are measured to demonstrate the resilience of Bessel beams in the presence of an opaque metallic obstacle in the line of sight.

1 Introduction

Bessel beams, introduced by Durnin in 1987 [1], are exact solutions of the Helmholtz equation and appear to defy one of the fundamental laws of physics: diffraction. However, the realization of truly non diffractive beams would need an infinitely large aperture and, since Bessel beams are not square integrable functions, an infinite amount of energy. Fortunately, one can generate truncated or tapered Bessel distributions, which exhibit non diffractive behavior within a limited range referred to as the non diffractive range (NDR).

Bessel beams have primarily been investigated in optics and applied to areas such as optical tweezers [2], laser machining [3], or even ultrasound imaging [4]. They are typically generated using an axicon lens fed by a Gaussian beam. Their non-diffractive property can be understood through ray optics, as they do not produce a focal point like traditional lenses but instead create a line-shaped focus. In addition to their non diffractive properties, these beams can reconstruct themselves after passing through a shadow region caused by an obstructing opaque metallic obstacle.

Due to the constant increase in the data rates required for short-range connections for Wireless Personal Area Networks (WPANs), kiosk downloading, future data centers [5], and wireless energy transfer [6, 7], millimeter-wave Bessel beams [8–11] are garnering growing interest. At microwave and millimeter-wave frequencies, Bessel beam launchers based on conventional lenses either experience spillover losses due to their limited electrical size or become excessively bulky. The solutions based on metasurfaces use radial waveguides and artificial surfaces, providing compact structures [8–12]. However, their resonant or dispersive properties imply a relatively limited bandwidth, generally less than 20%. We propose a relatively compact Bessel beam former based on a W-band spline-curved horn with a 33% relative bandwidth, ranging from 75 GHz to 105 GHz. This non-diffractive source is then used to establish high-speed near-field connections resilient to obstructions.

This paper is structured as follows: Section 2 comprehensively describes our broadband W-band Bessel-beam launcher. Section 3 details the microwave photonics link setup employed for our link demonstrations. In Section 4 we experimentally demonstrate the self-healing property by featuring Bit Error Rate (BER) measurements both with and without an opaque metallic obstacle obstructing the LOS. Finally, Section V draws the conclusions.

2 Bessel beam launcher

The non-diffractive Bessel beams are generated by means of a spline-profile horn, which presents a circular radiating aperture with radius r of 15 mm ($4.5\lambda_0$, with λ_0 being the free space wavelength at the central operating frequency of 90 GHz).

The non-diffractive behavior [9] is obtained by synthesizing the higher-order TE_{02} transverse electric mode of a circular aperture [13]. Thus, the tangential aperture field reads as:

$$E_\phi = E_0 k_0 \eta J_1(k_c \rho) \tag{1}$$

with E_0 being an arbitrary complex-valued constant, and k_0 and η the free space wavenumber and impedance, respectively. $J_1(\cdot)$ is the Bessel function of first kind and first order and k_c stands for the radial wavenumber of the generated Bessel beam. The radial wavenumber k_c is fixed to $j_{12}/r = 0.25\,k_0$, where j_{nm} is the m-th root of $J_n(\cdot)$ ($j_{12} = 7.016$ in our case). The value of k_c yields a Bessel beam with a

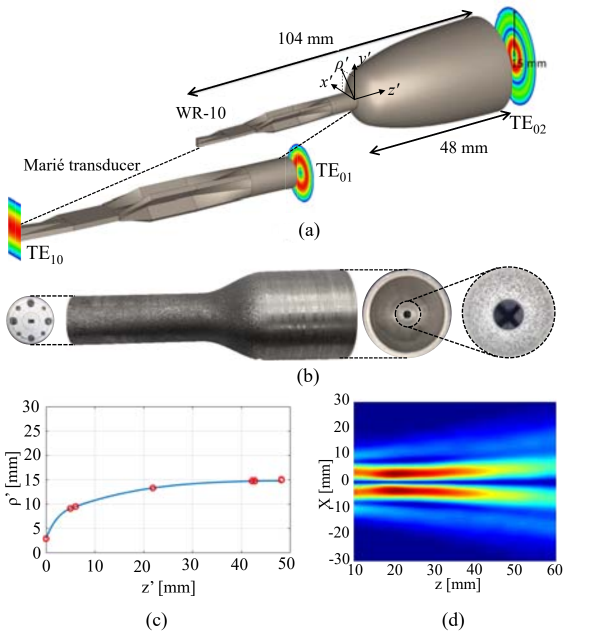

Figure 1. (a) Internal shape of the horn as well as the modal amplitudes at the input of the rectangular WR-10 waveguide and at the output of the circular waveguides. (b) Picture of the Bessel beam former. (c) Spline-profile section of the transmitter, circular markers determine the position of control points; ρ' represents the radial coordinate. (d) Amplitude of the electric field $|E_\phi|$ measured in the xoz plane at 90 GHz.

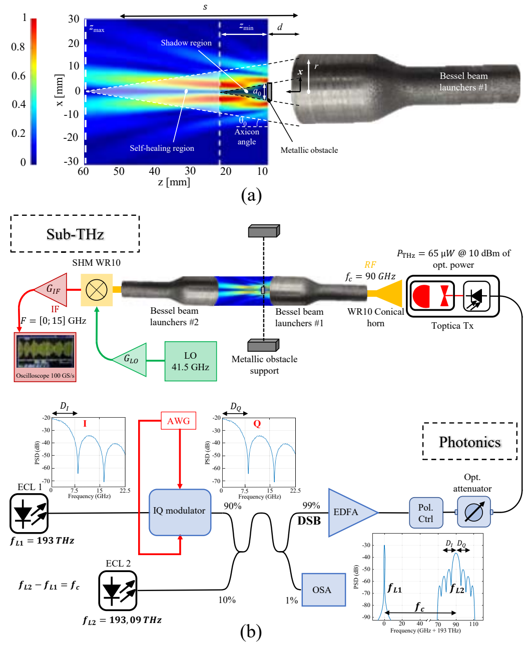

Figure 2. (a) Normalized electric field magnitude E_ϕ in the xoz plane measured at 90 GHz with a metallic obstacle in the LOS located at $d = 9.6$ mm (b) Coherent opto-electronic detection scheme. ECL: External Cavity Laser, DSB: Double Side Band, EDFA: Erbium Doped Fiber Amplifier, OSA: Optical Spectrum Analyser, Pol. Ctrl: Polarization Controler, AWG : Arbitrary Waveform Generator, NDR: Non Diffractive Range, SHM: Mixer, LO: Local Oscillator.

small axicon angle θ_0 ($\theta_0 = \arcsin(k_c/k_0) \approx 15°$) and, thus, a moderate non-diffractive range $z_{\max}$ given by [1]:

$$z_{\max} = r\sqrt{\left(\frac{k_0}{k_c}\right)^2 - 1} = r\cot\theta_0 \qquad (2)$$

The structure adopted to obtain the TE_{02} field distribution consists of two parts: a Marié mode converter and a spline-profile horn. The inset in Fig. 1(a) shows our Marié transducer [14, 15], which transforms the TE_{10} mode of a standard WR-10 rectangular waveguide into the higher-order TE_{01} circular waveguide mode. The Marié section provides the desired azimuthal symmetry at the input of the spline horn. As for the spline horn, it synthesizes the TE_{02} distribution over the radiating aperture in the 75–105 GHz band. The design relies on a optimization procedure [16], which is based on an in-house mode-matching tool and aims at converting the TE_{01} mode of an input circular waveguide with radius $\rho_{\text{in}} = 2.92$ mm to the targeted TE_{02} mode. To that end, the cubical spline profile is modified at each iteration by tuning the position of 7 control points defined in Fig. 1(c). The launcher has been fabricated using Selective Laser Melting (SLM) technology and AlSi10Mg powder material. Fig. 1(b) shows one of the realized launchers with insets that zoom in on both the WR-10 input waveguide and the output of the Marié converter.

The non diffractive range $z_{\max} = 60$ mm, as obtained from (2), has been experimentally verified at 90 GHz by measuring the electric-field magnitude $|E_\phi|$ in the xoz (see Fig. 1(d)).

3 Coherent near-field transmission setup

The sub-THz carrier can be generated either through an electronic approach, by up-conversion [17], or through a heterogeneous approach using optoelectronics to convert a waveform in the optical domain to the desired mm-wave frequency [18]. The latter approach was chosen for our near-field link due to the numerous advantages and flexibility in frequency selection offered by photonic technologies.

Figure 2(b) illustrates the transmission scheme adopted to achieve a coherent communication using a QPSK waveform at W-band. Two external-cavity lasers (ECL) are first used to generate two optical carriers at $f_{L1} = 193$ THz and $f_{L2} = 193.09$ THz, respectively. ECL1 is then modulated using a QPSK waveform. Finally, these two optical carriers are injected into a wideband THz photo-mixing transmitter from TOPTICA Photonics, which comprises a bowtie antenna driven by a PIN photodiode and placed at the focus of a hyper-hemispherical silicon lens [19].

The carrier is coupled into the Bessel beam former Tx us-

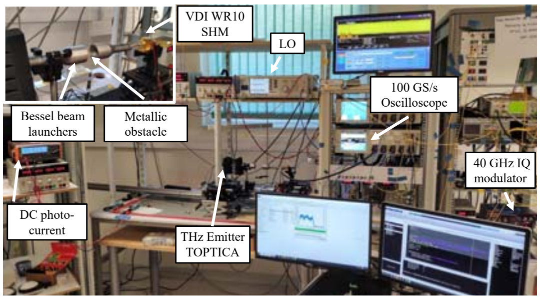

Figure 3. Pictures of the setup used for the BER measurements. Upper left: Zoom into the two Bessel beam launchers in the presence of a metallic obstacle.

ing a 20 dBi conical horn. The near-field link is established between two identical Bessel beam formers, as shown in Fig. 3. After being received by the second horn, the 90 GHz signal is down-converted to an intermediate frequency (IF) using a sub-harmonic mixer (VDI WR10 SHM) pumped at f_{LO}= 41.5GHz. The signal is then detected and recorded by an oscilloscope at a central frequency of 7GHz for offline IF demodulation.

4 Link measurements results

To illustrate the self-healing characteristic of the generated Bessel beams over the bandwidth of interest in a realistic scenario, we have compared the BER at 2.75 Gb/s while varying the distance between two Bessel-beam launchers, both with and without an opaque obstacle obstructing the Line Of Sight (LOS). The obstacle consists of a circular metallic patch with diameter $a_0 = 7$ mm and thickness $t = 0.42$ mm. The patch is axially aligned with the spline horn at a distance $d = 9.6$ mm from its aperture, using a thin dielectric thread and a 4-axis micropositioner (see Fig.3). The Bessel beam is expected to reconstruct itself after passing through a shadow depth $z_{\min}$, calculated using [20]:

$$z_{\min} = (a_0/2)\cot\theta_0. \tag{3}$$

For the selected obstacle, the estimation of the shadow depth using (3) yields $z_{\min} = 13.67$ mm at 90 GHz, a value experimentally confirmed by the measurements of the electric field magnitude E_ϕ, as shown in Fig. 2(a).

In the absence of an obstacle, error-free transmission was achieved in the range of 15 mm $< s <$ 115 mm. When an obstacle was placed at $d = 9.6$ mm, error-free transmission was obtained in the range of 25 mm $< s <$ 115 mm, which is in agreement with the previous case with an offset corresponding to slightly less than the shadow region. The BER curves in Fig. 4 can be divided into three regions. In the first few millimeters, i.e., 0 mm $< s <$ 15 mm, the BER is mostly limited by the presence of strong standing waves extinguishing the sub-mm carrier. At greater separations, $s >$ 35 mm, the standing wave effect becomes negligible

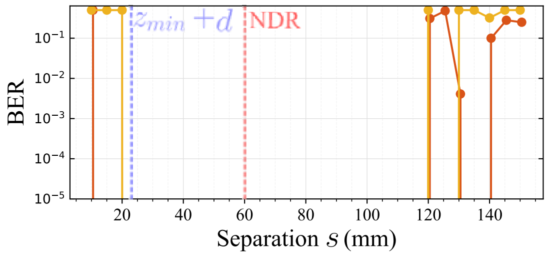

Figure 4. BER as a function of the separation s of the Bessel launchers using QPSK modulation format at 2.75 Gb/s. The red curves represents the BER w/o obstacle in the LOS and the yellow curve with an obstacle placed at $d = 9.6$ mm from the Tx Bessel launcher. The NDR is set at 60 mm and $z_{min} + d$ at 23 mm.

(less than 1 dB in our bandwidth of interest), until reaching the best Signal-to-Noise Ratio (SNR) at a distance of 50 mm. Beyond the NDR, which extends to approximately 60 mm at 90 GHz, the signal diminishes until the SNR becomes too low for reliable demodulation.

To further demonstrate the capability of our Bessel-beam launchers in achieving high data rates in near-field links, we placed the two Bessel-beam launchers at a distance $s = 60$ mm. This configuration was selected to optimize the transmitted power from the transmitter (Tx) to the receiver (Rx), achieving an estimated transmission coefficient ($|S_{21}|$, measured from the WR-10 input of launcher #1 to the WR10 output of launcher #2) higher than -4 dB across the entire bandwidth of interest. In this configuration, we successfully achieved a net data bitrate of 15.5 Gb/s using QPSK modulation by employing an advanced demodulation algorithm capable of compensating for the substantial power variations stemming from the TOPTICA module. Fig.5(a) shows the retrieved constellation, which corresponds to an Error Vector Magnitude of 18.7%. The associated normalized Power Spectrum Density (PSD) is depicted in orange in Fig. 5(b) with an SNR of 25 dB. The waveform bandwidth of 8 GHz reflects the spectral efficiency of 1.8 bits/Hz associated with the utilized modulation format.

We must emphasize that the achievable data rate with our Bessel beam formers can easily surpass the reported 15.5 Gb/s. Although the Toptica module can transmit up to 1.2 THz, the strong variations in emitted power over the frequency significantly impact the performance of the link, as illustrated by the dashed gray curve in Fig. 5(b), representing the normalized power variations of the Toptica transmitter in the considered frequency band.

5 Conclusion

This study demonstrates the robustness of millimeter-wave Bessel beams against strongly diffracting obstacles, confirming their ability to provide high throughput and reliability. Using two wideband transmitters from our laboratory, we illustrated the resilience of obstructed Bessel beams by

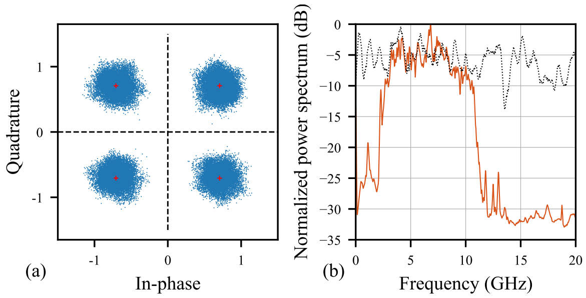

Figure 5. (a) Constellation diagram of QPSK waveform at 15.5 Gb/s. (b) Orange curve : Associated normalized Power Spectrum Density of the received QPSK waveform. Grey dotted curve: Measured emitted power of the Toptica Tx photo-mixer reported at IF frequencies (0–20 GHz).

a 7 mm metallic obstacle at a distance of 9.6 mm, analyzing the BER at 2.75 Gb/s with and without the obstacle. An offline QPSK link at 15.5 Gb/s (BER $< 10^{-5}$) was established, highlighting the potential of sub-millimeter-wave Bessel beams to address challenges in near-field communications and pave the way for practical applications in high-speed wireless communication systems.

6 Acknowledgement

This work has been supported by the European Union through European Regional Development Fund (ERDF), Ministry of Higher Education and Research, CNRS, Brittany region, Conseils Départementaux d'Ille-et-Vilaine and Côtes d'Armor, Rennes Métropole, and Lannion Trégor Communauté, through the CPER Projects CyMoCod and Phot-Breizh. This work has received a French government support granted to the Labex CominLabs excellence laboratory and managed by the National Research Agency in the "Investing for the Future" program under reference ANR-10-LABX-07-01 and program WASSAP.

References

[1] J. Durnin, "Exact solutions for nondiffracting beams. I. The scalar theory," *J. Opt. Soc. Am. A*, vol. 4, no. 4, pp. 651–654, Apr 1987.

[2] V. Garcés-Chávez, D. McGloin, H. Melville, W. Sibbett, and K. Dholakia, "Simultaneous micromanipulation in multiple planes using a self-reconstructing light beam," *Nature*, vol. 419, no. 6903, pp. 145–147, Sep. 2002.

[3] Y. Matsuoka, Y. Kizuka, and T. Inoue, "The characteristics of laser micro drilling using a bessel beam," *Appl. Phys. A*, vol. 84, no. 4, pp. 423–430, Sep 2006.

[4] J.-Y. Lu, X.-L. Xu, H. Zou, and J. Greenleaf, "Application of Bessel beam for Doppler velocity estimation," *IEEE Trans. Ultrason. Ferroelectr. Freq. Control*, vol. 42, no. 4, pp. 649–662, 1995.

[5] T. Kürner and S. Priebe, "Towards THz communications - status in research, standardization and regulation," *J. Infra. Millim. Terahz Waves*, vol. 35, no. 1, pp. 53–62, Jan 2014.

[6] S. Paković, S. Zhou, D. González-Ovejero, S. C. Pavone, A. Grbic, and M. Ettorre, "Bessel–Gauss beam launchers for wireless power transfer," *IEEE Open J. Antennas Propag.*, vol. 2, pp. 654–663, 2021.

[7] E. Negri, W. Fuscaldo, P. Burghignoli, and A. Galli, "Leaky-wave analysis of tm-, te-, and hybrid-polarized aperture-fed bessel-beam launchers for wireless-power-transfer links," *IEEE Trans. Antennas Propag.*, vol. 71, no. 2, pp. 1424–1436, 2022.

[8] M. Albani, S. C. Pavone, M. Casaletti, and M. Ettorre, "Generation of non-diffractive Bessel beams by inward cylindrical traveling wave aperture distributions," *Opt. Express*, vol. 22, no. 15, pp. 18 354–18 364, Jul 2014.

[9] M. Ettorre, S. M. Rudolph, and A. Grbic, "Generation of propagating Bessel beams using leaky-wave modes: Experimental validation," *IEEE Trans. Antennas Propag.*, vol. 60, no. 6, pp. 2645–2653, 2012.

[10] W. Fuscaldo, G. Valerio, A. Galli, R. Sauleau, A. Grbic, and M. Ettorre, "Higher-order leaky-mode Bessel-beam launcher," *IEEE Trans. Antennas Propag.*, vol. 64, no. 3, pp. 904–913, 2016.

[11] S. C. Pavone, M. Ettorre, M. Casaletti, and M. Albani, "Analysis and design of Bessel beam launchers: Transverse polarization," *IEEE Trans. Antennas Propag.*, vol. 69, no. 8, pp. 5175–5180, 2021.

[12] M. Ettorre and A. Grbic, "Generation of propagating Bessel beams using leaky-wave modes," *IEEE Trans. Antennas Propag.*, vol. 60, no. 8, pp. 3605–3613, 2012.

[13] D. M. Pozar, *Microwave Engineering*, 4th ed. Hoboken, NJ: John Wiley & Sons, 2012.

[14] S. Saad, J. Davies, and O. Davies, "Analysis and design of a circular TE_{01} mode transducer," *IEE J. Microw., Opt. Acoust.*, vol. 1, no. 2, pp. 58–62, 1977.

[15] M. González-Calvo, J. R. Montejo-Garai, J. A. Ruiz-Cruz, and J. M. Rebollar, "Additive manufacturing of a high-performance Q-band circular TE_{01} mode flared-type transducer," *IEEE Microw. Wireless Compon. Lett.*, vol. 29, no. 9, pp. 577–579, 2019.

[16] S. Paković, N. Bartolomei, M. J. Mencagli, M. Ettorre, R. Sauleau, and D. González-Ovejero, "A fast and accurate method of synthesizing X-wave launchers by metallic horns," *IEEE Access*, vol. 9, pp. 1996–2006, 2021.

[17] A. Karakuzulu, W. A. Ahmad, D. Kissinger, and A. Malignaggi, "A four-channel bidirectional d-band phased-array transceiver for 200 Gb/s 6G wireless communications in a 130-nm BiCMOS technology," *IEEE J. Solid-State Circuits*, vol. 58, no. 5, pp. 1310–1322, 2023.

[18] T. Nagatsuma, G. Ducournau, and C. C. Renaud, "Advances in terahertz communications accelerated by photonics," *Nature Photon.*, vol. 10, no. 6, pp. 371–379, Jun. 2016.

[19] S. Nellen, S. Lauck, G. Schwanke, M. Deumer, R. B. Kohlhaas, L. Liebermeister, M. Schell, and B. Globisch, "Radiation pattern of planar optoelectronic antennas for broadband continuous-wave terahertz emission," *Opt. Express*, vol. 29, no. 6, pp. 8244–8257, Mar 2021.

[20] Z. Bouchal, J. Wagner, and M. Chlup, "Self-reconstruction of a distorted non-diffracting beam," *Opt. Commun.*, vol. 151, no. 4, pp. 207–211, 1998.